Available online at www.sciencedirect.com
ScienceDirect
Comput. Methods Appl. Mech. Engrg. 278 (2014) 479–498
Computer methods in applied mechanics and engineering
www.elsevier.com/locate/cma

Direct meshless local Petrov–Galerkin method for elliptic interface problems with applications in electrostatic and elastostatic

Ameneh Taleei, Mehdi Dehghan*

Department of Applied Mathematics, Faculty of Mathematics and Computer Science, Amirkabir University of Technology, No. 424, Hafez Ave., 15914, Tehran, Iran

Received 27 January 2014; received in revised form 3 May 2014; accepted 26 May 2014
Available online 5 June 2014

Abstract

In recent years, there have been extensive efforts to find the numerical methods for solving problems with interface. The main idea of this work is to introduce an efficient truly meshless method based on the weak form for interface problems. The proposed method combines the direct meshless local Petrov–Galerkin method with the visibility criterion technique to solve the interface problems. It is well-known in the classical meshless local Petrov–Galerkin method, the numerical integration of local weak form based on the moving least squares shape function is computationally expensive. The direct meshless local Petrov–Galerkin method is a newly developed modification of the meshless local Petrov–Galerkin method that any linear functional of moving least squares approximation will be only done on its basis functions. It is done by using a generalized moving least squares approximation, when approximating a test functional in terms of nodes without employing shape functions. The direct meshless local Petrov–Galerkin method can be a very attractive scheme for computer modeling and simulation of problems in engineering and sciences, as it significantly uses less computational time in comparison with the classical meshless local Petrov–Galerkin method. To create the appropriate generalized moving least squares approximation in the vicinity of an interface, we choose the visibility criterion technique that modifies the support of the weight (or kernel) function. This technique, by truncating the support of the weight function, ignores the nodes on the other side of the interface and leads to a simple and efficient computational procedure for the solution of closed interface problems. In the proposed method, the essential boundary conditions and the jump conditions are directly imposed by substituting the corresponding terms in the system of equations. Also, the Heaviside step function is applied as the test function in the weak form on the local subdomains. Some numerical tests are given including weak and strong discontinuities in the Poisson interface problem. To demonstrate the application of these problems, linearized Poisson–Boltzmann and linear elasticity problems with two phases are studied. The proposed method is compared with analytical solution and the meshless local Petrov–Galerkin method on several test problems taken from the literature. The numerical results confirm the effectiveness of the proposed method for the interface problems and also provide significant savings in computational time rather than the classical meshless local Petrov–Galerkin method.

MSC: 82B24; 35J05; 35J57; 35Q74

Keywords: Meshless method; Generalized moving least squares (GMLS) approximation; Direct Meshless local Petrov–Galerkin (DMLPG) method; Scalar potential and elasticity interface problems; Linearized Poisson–Boltzmann equation; Visibility criterion technique

* Corresponding author. Tel.: +98 21 64542503.
E-mail addresses: ataleei@aut.ac.ir (A. Taleei), mdehghan@aut.ac.ir, mdehghan.aut@gmail.com (M. Dehghan).

http://dx.doi.org/10.1016/j.cma.2014.05.016
0045-7825/

1. Introduction

Many important physical and industrial applications involve mathematical models with very complicated structure that are characterized by discontinuous or even singular material properties. These problems are known as interface problems. Interface problems arise in various branches of sciences and engineering such as biological systems and material sciences [1]. Electrostatics play a key role in many biological processes. The Poisson–Boltzmann equation is one of the most popular models for describing electrostatic interactions between molecules in ionic solutions. This equation and its linearized form allow prediction of electrostatic effects for biomolecular systems [2]. Elasticity problems of multiple phase elastic materials separated by phase interfaces often arise in material science [3–6]. They have wide applications in continuum mechanics, particularly for problems that include stresses and strains. Two important examples of such problems occur in the microstructural evolution of precipitates in an elastic matrix due to the diffusion of concentration and in the morphological instability due to stress-driven surface diffusion in solid thin films [7,8]. The understanding of these physical processes is crucial to improve material stability properties and in turn to develop new and advanced materials that have applications in automobile manufacture, aircraft industries and modern communication technologies. For various applications in real world problems, recently there have been great efforts to develop efficient and accurate techniques [9–11].

In recent years, there have been extensive efforts to find numerical methods for the solution of interface problems. The development of meshless methods and also, the mesh-based methods such as the extended finite element method (XFEM) leads to the solutions of interface problems without remeshing [12]. It is well-known that the integration of weak form in meshless methods has bigger challenge than the XFEM. It should be noted that the stiffness matrix in XFEM is usually constructed by integrating over polynomial basis functions and it is much cheaper to evaluate but it is usually a tedious procedure, especially in high dimensional problems, if the curved interface is more complex.

Meshless methods [13–17] are very attractive and effective for solving boundary value problems, because they involve simple preprocessing, arbitrary node distribution and flexibility of placing nodes at arbitrary locations, straightforward adaptive refinement, versatility in solving large deformation and also have the high order continuity and the ability to treat the evolution of non-smooth solutions, which is very useful to solve the interface problems. Many of them are derived from a weak-form formulation on a global domain or a set of local subdomains. The integration of the local weak-form, unlike the global weak-form, does not need any background integration cells over the entire domain. One of the most efficient meshless local weak-form methods is the meshless local Petrov–Galerkin (MLPG) method based on the moving least squares (MLS) approximation introduced by Atluri and Zhu [18].

Atluri and Shen [19] discussed the MLPG method based on symmetric and unsymmetric weak forms with different types of meshless interpolations for trial and test functions. They derived six MLPG formulations depending on various test functions and marked by MLPG1–MLPG6. The success of the MLPG method has been reported in solving several engineering problems (see [20–22] and the references therein).

In the meshless methods based on MLS, the smoothness of the shape functions is determined by that of the basis functions and the weight functions [23]. However, the employment of smooth approximation near interface leads to a difficulty in handling problems with discontinuities in the solution or its derivatives [24]. To obtain accurate discontinuous solutions using meshless methods, several different approaches have been proposed (see [23–37]). An efficient and simple technique is the visibility criterion scheme that the support domain of the shape function or approximation function is cut by the interface [23,26]. This technique leads to a proper approximation near the closed interface problems.

A variety of MLPG methods has been applied to interface problems. Batra et al. [25] studied the heat conduction in a bimetallic circular disk with homogeneous jump conditions by MLPG1 and MLPG5. Nicomedes et al. [38,39] employed MLPG4 for the study of electromagnetic problems. Li et al. [31] investigated the combination of MLPG2 and MLPG5 for the solution of three-dimensional elastostatic problem with homogeneous jump conditions. Among the meshless local Petrov–Galerkin methods with weak form, MLPG5 or MLPG with a Heaviside step function as a test function is computationally less expensive [19]. This method has been successfully applied to multi-field coupled and crack problems [40–42].

The method of MLS is generally considered as a beneficial scheme to approximate discrete data with a reasonable accuracy. However, it has some disadvantages. One of the most important drawbacks of this method is the computational cost which is caused by the required CPU time to calculate the derivative and especially the integration of MLS shape functions. Recently, a new class of MLPG methods, known as the direct meshless local Petrov–Galerkin

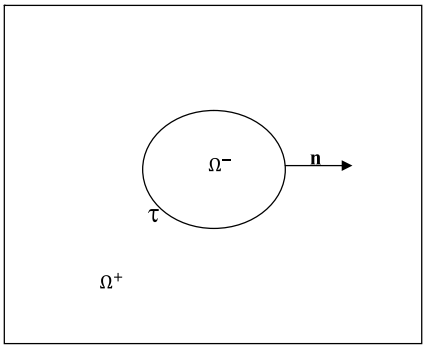

Fig. 1. A rectangular domain Ω with the interface τ.

(DMLPG) method, has been developed by Mirzaei and Schaback [43]. In the DMLPG method, the generalized moving least squares (GMLS) approximation [44] recovers test functionals directly from values at nodes, without any detour via shape functions. In particular, the complete absence of shape functions allows numerical integration in the weak form of the problem to be done over low-degree polynomials instead of complicated shape functions. This method has been employed to solve the Poisson equation [43] and the transient heat conduction equation [45]. They have shown it requires less computational effort than MLPG. Also Mazzia et al. [46] studied this method for 2D and 3D potential problems.

In this work, we intend to study the DMLPG method with visibility criterion technique for the closed interface boundary value problems. To the authors' best knowledge, this is the first study of the DMLPG technique for the numerical solution of interface problems. These problems include the scalar potential interface problems and also the two-phase elasticity system which is the application of these problems to vector form. For these two-phase boundary value problems, jump conditions across the interface can be homogeneous or nonhomogeneous. In this paper, we investigate the scalar potential interface problem with homogeneous and nonhomogeneous jump conditions. We also study the linearized Poisson–Boltzmann equation with different dielectric constants and the elasticity problem that can arise from several modeling situations such as two-phase elastic plates in the setting of plane strain or plane stress. In order to show the advantages of truly meshless technique for the proposed method a complex interface with regular and irregular node distributions is also tested.

The rest of the paper is organized as follows: Section 2, gives the interface model of scalar and vector potential problems and presents the local weak formulation for these interface problems. In Section 3, we describe DMLPG based on GMLS with weight modification for the interface problems. We discuss how to construct the approximation of an unknown solution for these interface problems. Firstly, the proposed method is explained for scalar potential interface problem and then it is extended to the elasticity problem. Some examples are presented to show the performance of the proposed technique in Section 4. We provide numerical experiments to confirm that the DMLPG method with the visibility criterion technique can effectively solve the interface problems. Section 5 completes this paper with concluding remarks.

2. Mathematical formulation

Let Ω be a convex domain with Lipschitz continuous boundary in $\mathbb{R}^2$, which is separated into two disjoint subregions Ω^+ and Ω^- by the interface τ, i.e. $\Omega = \Omega^+ \cup \Omega^- \cup \tau$, where τ is a closed interface [12], thus it does not pass the origin within the domain (see Fig. 1 for a geometric illustration). Also the vector $\mathbf{n} = (n_1, n_2)$ is the unit normal direction of τ pointing from the Ω^- phase to the Ω^+ phase or pointing outward to the boundary. In the following, we will illustrate scalar potential and elasticity problems with closed interface and obtain their local weak formulations.

2.1. The scalar potential interface problem

Consider the two-dimensional elliptic equation as follows

$$-\nabla \cdot (\beta \nabla u) + k^2 u = f \quad \text{in } \Omega^{\pm}, \tag{2.1}$$

$$u = g, \quad \text{on } \partial\Omega, \tag{2.2}$$

where f is taken as given scalar field that may be discontinuous across the interface with the jump conditions on the interface:

$$[u]_\tau(\mathbf{x}) \equiv u^+(\mathbf{x}) - u^-(\mathbf{x}) = j_1(\mathbf{x}), \quad \text{on } \tau, \tag{2.3}$$

$$\left[\beta \frac{\partial u}{\partial \mathbf{n}_\tau}\right]_\tau (\mathbf{x}) \equiv \beta^+ \frac{\partial u^+}{\partial \mathbf{n}_\tau}(\mathbf{x}) - \beta^- \frac{\partial u^-}{\partial \mathbf{n}_\tau}(\mathbf{x}) = j_2(\mathbf{x}), \quad \text{on } \tau. \tag{2.4}$$

The coefficients β and k can be also discontinuous across the interface τ, i.e.

$$\beta(\mathbf{x}) = \begin{cases} \beta^+(\mathbf{x}), & \mathbf{x} \in \Omega^+, \\ \beta^-(\mathbf{x}), & \mathbf{x} \in \Omega^-, \end{cases}$$

$$k(\mathbf{x}) = \begin{cases} k^+(\mathbf{x}), & \mathbf{x} \in \Omega^+, \\ k^-(\mathbf{x}), & \mathbf{x} \in \Omega^-. \end{cases}$$

The above equation is the linearized Poisson–Boltzmann equation in the case of weak electrostatic potential, where k absorbs all the related parameters, and f and u are the scaled singular charge distribution and electrostatic potential, respectively [47]. Also β and ∇u represent the position-dependent dielectric and the gradient of the electrostatic potential, respectively [2]. To find a weak formulation for the above interface problem, we multiply (2.1) by test function v and integrate on both subregions Ω^+ and Ω^-. Applying Green's theorem in the domain Ω^+, outside of the closed interface τ, we get

$$-\int_{\partial\Omega^+\setminus\tau} \beta \frac{\partial u}{\partial \mathbf{n}} v d\Gamma - \int_\tau \beta^+ \frac{\partial u^+}{\partial \mathbf{n}_\tau^+} v d\Gamma + \int_{\Omega^+} \beta \nabla u \cdot \nabla v d\Omega + \int_{\Omega^+} k^2 u v d\Omega = \int_{\Omega^+} f v d\Omega. \tag{2.5}$$

Similarly, we have the following relation from the inside of the interface, i.e., Ω^-

$$-\int_{\partial\Omega^-\setminus\tau} \beta \frac{\partial u}{\partial \mathbf{n}} v d\Gamma - \int_\tau \beta^- \frac{\partial u^-}{\partial \mathbf{n}_\tau^-} v d\Gamma + \int_{\Omega^-} \beta \nabla u \cdot \nabla v d\Omega + \int_{\Omega^-} k^2 u v d\Omega = \int_{\Omega^-} f v d\Omega. \tag{2.6}$$

Since $\mathbf{n}_\tau^- = -\mathbf{n}_\tau^+ = \mathbf{n}_\tau$ and adding (2.5) and (2.6) together, we get

$$-\int_{\partial\Omega} \beta \frac{\partial u}{\partial \mathbf{n}} v d\Gamma + \int_\Omega \beta \nabla u \cdot \nabla v d\Omega + \int_\Omega k^2 u v d\Omega = \int_\Omega f v d\Omega - \int_\tau j_2 v d\Gamma. \tag{2.7}$$

Hence, the weak form of the interface boundary value problem (2.1)–(2.4) is:

$$\text{Find } u \in \mathcal{U} \text{ such that } a(u, v) = (f, v); \quad \forall v \in \mathcal{V},$$

$$a(u, v) = -\int_{\partial\Omega} \beta \frac{\partial u}{\partial \mathbf{n}} v d\Gamma + \int_\Omega \beta \nabla u \cdot \nabla v d\Omega + \int_\Omega k^2 u v d\Omega,$$

$$(f, v) = \int_\Omega f v d\Omega - \int_\tau j_2 v d\Gamma,$$

where $\mathcal{U}$ and $\mathcal{V}$ are the trial and test spaces, respectively. The functions in $\mathcal{U}, \mathcal{V} \subset H^1(\Omega^+ \cup \Omega^-)$ satisfy in the boundary condition (2.2) and jump conditions (2.3)–(2.4).

The DMLPG method is used to find the numerical solution of the boundary value problems using the local weak-form formulation. In the sequel we consider a weak form over the local fictitious subdomains such as Ω_q, which is a small region taken for each node inside the subregion domains $\Omega^\pm$. These test domains could be of any geometrical shape and size. In the present paper, the test domain Ω_q is chosen as a circle, centered at an interior node $\mathbf{x}_i$.

A local weak form can be obtained for each test domain $\Omega_q^\pm$ as follows

$$-\int_{L_q^\pm \cup \Gamma_{qu}^\pm \cup \Gamma_{qt}^\pm} \beta \frac{\partial u}{\partial \mathbf{n}} v d\Gamma - \int_{\Gamma_{q\tau}^\pm} \beta \frac{\partial u}{\partial \mathbf{n}_\tau} v d\Gamma + \int_{\Omega_q^\pm} \beta \nabla u \cdot \nabla v d\Omega + \int_{\Omega_q^\pm} k^2 u v d\Omega = \int_{\Omega_q^\pm} f v d\Omega, \tag{2.8}$$

where $\partial\Omega_q^\pm$ is the boundary of the local subdomain, which consists of four parts $\partial\Omega_q^\pm = L_q^\pm \cup \Gamma_{qt}^\pm \cup \Gamma_{qu}^\pm \cap \Gamma_{q\tau}^\pm$, in general. Here, $L_q^\pm$ is the local boundary that is totally located inside the subregions Ω^+ or Ω^-, $\Gamma_{qt}^\pm$ is the part of the

local boundary that coincides with the global Neumann boundary, that is, $\Gamma_{qt}^{\pm} = \partial\Omega_q^{\pm} \cap \partial\Omega_t$, and similarly $\Gamma_{qu}^{\pm}$ is the part of the local boundary that coincides with the global Dirichlet boundary, that is, $\Gamma_{qu}^{\pm} = \partial\Omega_q^{\pm} \cap \partial\Omega_u$. Also, $\Gamma_{q\tau}^{\pm}$ is the part of the local boundary that coincides with interface τ, that is, $\Gamma_{q\tau}^{\pm} = \partial\Omega_q^{\pm} \cap \tau$. We assume that the local subdomains around interior nodes do not cross the interface and the global boundary, thus the local weak form (2.8) is converted into the following form

$$-\int_{L_q^{\pm}} \beta \frac{\partial u}{\partial \mathbf{n}} v d\Gamma + \int_{\Omega_q^{\pm}} \beta \nabla u \cdot \nabla v d\Omega + \int_{\Omega_q^{\pm}} k^2 u v d\Omega = \int_{\Omega_q^{\pm}} f v d\Omega. \tag{2.9}$$

2.2. The elasticity interface problem

In the following, we consider the elasticity system that the material coefficients may have finite jumps across the interface τ [11,31,48]: It is governed by

$$\nabla \cdot \boldsymbol{\sigma}(\mathbf{u}) + \mathbf{f} = 0, \quad \text{in } \Omega^{\pm}, \tag{2.10}$$

$$\mathbf{u} = \mathbf{u}_D, \quad \text{on } \partial\Omega, \tag{2.11}$$

where $\boldsymbol{\sigma}(\mathbf{u})$ is the stress tensor, $\mathbf{f} = (f_1, f_2)^T$ is the body force and $\mathbf{u} = (u_1, u_2)^T$ is the displacement field. We assume that the material is isotropic. So, in the setting of plane deformation, the stress–strain relation is given by

$$\boldsymbol{\sigma}(\mathbf{u}) = \lambda \operatorname{tr}(\boldsymbol{\epsilon}(\mathbf{u}))\mathbf{I} + 2\mu\boldsymbol{\epsilon}(\mathbf{u}), \tag{2.12}$$

where $\boldsymbol{\epsilon}(\mathbf{u}) = \frac{1}{2}(\nabla\mathbf{u} + (\nabla\mathbf{u})^T)$ is the linear strain, $\mathbf{I}$ is the 2×2 identity tensor. Also, the Lamé constants [5] μ and λ are as

$$\mu = \frac{E}{2(1+\nu)},$$

and

$$\lambda = \begin{cases} \dfrac{E\nu}{(1+\nu)(1-2\nu)}, & \text{(plane strain)}, \\ \dfrac{E\nu}{1-\nu^2}, & \text{(plane stress)}, \end{cases}$$

where, E is Young's modulus, and ν is Poisson's ratio. Note that, in practice, it is common to use the Young's modulus E and Poisson's ratio ν instead of the Lamé coefficients λ and μ in the expression (2.12). In modeling a two-phase elastic material, we assume that all the material parameters μ, λ, E and ν are piecewise constants. The physical parameters such as Lamé constants may have a finite discontinuity across the interface τ, i.e.,

$$(\mu, \lambda) = \begin{cases} (\mu^+, \lambda^+), & \text{on } \Omega^+, \\ (\mu^-, \lambda^-), & \text{on } \Omega^-, \end{cases}$$

where all μ^+, μ^-, λ^+ and λ^- are positive constants. Across the material interface τ, the displacement and traction are assumed to have the following jump conditions

$$[\mathbf{u}]_\tau = \mathbf{j}_1, \quad \text{on } \tau, \tag{2.13}$$

$$[\boldsymbol{\sigma}(\mathbf{u})\mathbf{n}]_\tau = \mathbf{j}_2, \quad \text{on } \tau. \tag{2.14}$$

In the following, we obtain the local weak form for the above planar elasticity interface problem that is actually an application of the potential interface problem in the vector mode.

To derive the local weak formulation of the elasticity system (2.10) over the subdomain Ω_q, using the divergence theorem, the following expression is obtained

$$\int_{\Omega_q^{\pm}} 2\mu\boldsymbol{\epsilon}(\mathbf{u}) : \boldsymbol{\epsilon}(\mathbf{v}) d\Omega + \int_{\Omega_q^{\pm}} \lambda(\nabla \cdot \mathbf{u})(\nabla \cdot \mathbf{v}) d\Omega - \int_{L_q^{\pm}} \boldsymbol{\sigma}(\mathbf{u})\mathbf{n} \cdot \mathbf{v} d\Gamma = \int_{\Omega_q^{\pm}} \mathbf{f} \cdot \mathbf{v} d\Omega, \tag{2.15}$$

in which the inner-product of two tensors is defined by

$$\boldsymbol{\epsilon}(\mathbf{u}) : \boldsymbol{\epsilon}(\mathbf{v}) = \sum_{i,j=1}^{2} \epsilon_{ij}(\mathbf{u})\epsilon_{ij}(\mathbf{v}). \tag{2.16}$$

The test vector function $\mathbf{v}$ is $\mathbf{v} = (v_1, v_2)$ and the test domain $\Omega_q^{\pm}$ is only associated to interior nodes. It should be noted that these test domains do not cross the interface and the global boundary.

3. Numerical method

In the original MLPG method based on MLS, trial functions and sometimes test functions are approximated by using the MLS approximation. But in the DMLPG method, corresponding to each local integral equation, a linear functional as test functional is considered. These linear functionals are approximated by GMLS. In the rest of this section, we first illustrate the GMLS approximation. Since to modify the approximation near the interface, the modification of the weight function is applied, therefore we introduce an efficient one among these techniques for closed interface, namely the visibility criterion [24]. At last, using a Heaviside step function as the test function in the DMLPG method, we obtain a system of discretized equations corresponding to the studied boundary value problems. To employ the DMLPG method, the obtained local weak forms are applied for interior nodes and also the boundary and jump conditions are directly imposed.

3.1. Generalized moving least squares (GMLS) approximation

In the classical MLS method, by minimizing a certain weighted discrete L_2-norm, the approximate value of the unknown function u at each node in the domain, i.e., $\mathbf{x} \in \Omega \subset \mathbb{R}^d$, is obtained by using the values $u(\mathbf{x}_j)$ at nodes $\{\mathbf{x}_j\}_{j=1}^N$. In GMLS which is developed by Mirzaei et al. [44], the approximate value of each linear functional of the unknown function u, i.e., $\lambda(u)$, is given by functionals $\{\gamma_j(u)\}_{j=1}^N$. The GMLS method approximates linear functionals that can describe, for instance, point evaluation of u or its derivatives. In the following, we recall the GMLS approximation.

Let u be a sufficiently smooth function, $u \in C^m(\Omega)$, that is defined on a simple connected set $\Omega \in \mathbb{R}^d$. Moreover, let $\{\gamma_j(u)\}_{j=1}^N$ be a set of continuous linear functional γ_j from the dual $C^m(\Omega)^*$ of $C^m(\Omega)$. For a fixed linear functional $\lambda \in C^m(\Omega)^*$, the GMLS method approximates the value of $\lambda(u)$ from the data set $\{\gamma_j(u)\}_{j=1}^N$. The approximation $\widehat{\lambda(u)}$ of $\lambda(u)$ is a linear function of $\gamma_j(u)$ as follows

$$\widehat{\lambda(u)} = \sum_{j=1}^{N} a_j(\lambda)\gamma_j(u), \tag{3.1}$$

where the coefficients a_j are linear in λ. This problem is solved under the assumption that, the approximation (3.1) to be exact for a finite dimensional subspace of $P_m^d = \text{span}\{p_1, p_2, \ldots, p_Q\}$, i.e.

$$\sum_{j=1}^{N} a_j(\lambda)\gamma_j(p) = \lambda(p), \quad p \in P_m^d, \tag{3.2}$$

in which P_m^d is the space of d-variate polynomials of degree at most m with dimension $Q = \frac{(m+d)!}{m!d!}$.

The GMLS approximation $\widehat{\lambda(u)}$ for $\lambda(u)$ is numerically obtained as $\widehat{\lambda(u)} = \lambda(p^*)$, where $p^* \in P_m^d$ minimizes the following functional

$$J := \left\{ \sum_{j=1}^{N} [\gamma_j(u) - \gamma_j(p)]^2 w(\lambda; \gamma_j) : p \in P_m^d \right\}, \tag{3.3}$$

where $w(\lambda; \gamma_j)$ are given non-negative weights [49]. The existence and uniqueness conditions for this problem are provided in Theorem 4.7 of Wendland [50].

Since $p \in P_m^d$, we can define $p(\mathbf{x})$ as follows

$$p(\mathbf{x}) = \sum_{i=1}^{Q} l_i p_i(\mathbf{x}). \tag{3.4}$$

Using Eq. (3.4) and the linearity of the functionals γ_j, we have

$$\gamma_j(p(\mathbf{x})) = \sum_{i=1}^{Q} l_i \gamma_j(p_i(\mathbf{x})) = \mathbf{p}_{\gamma_j}^T \boldsymbol{\ell}, \tag{3.5}$$

where $\mathbf{p}_{\gamma_j} = (\gamma_j(p_1), \ldots, \gamma_j(p_Q))^T$, $\boldsymbol{\ell} = (l_1, l_2, \ldots, l_Q)^T$. The functional (3.3) can be rewritten into

$$J(\boldsymbol{\ell}) := \sum_{j=1}^{N} w(\lambda; \gamma_j)(\gamma_j(u) - \mathbf{p}_{\gamma_j}^T \boldsymbol{\ell})^2. \tag{3.6}$$

By minimizing the quadratic functional $J(\boldsymbol{\ell})$, we will have $\boldsymbol{\ell}^*$ as follows

$$\boldsymbol{\ell}^* = (\mathbf{M}(\lambda; \gamma))^{-1} \mathbf{B}(\lambda; \gamma) \hat{\boldsymbol{\gamma}}(u), \tag{3.7}$$

where

$$\begin{aligned}
&\mathbf{M}(\lambda; \gamma) = \mathbf{P}_\gamma \mathbf{W}(\lambda; \gamma) \mathbf{P}_\gamma^T,\\
&\mathbf{B}(\lambda; \gamma) = \mathbf{P}_\gamma \mathbf{W}(\lambda; \gamma),\\
&\mathbf{P}_\gamma = (\mathbf{p}_{\gamma_1}, \mathbf{p}_{\gamma_2}, \ldots, \mathbf{p}_{\gamma_N}),\\
&\mathbf{W}(\lambda; \gamma) = \operatorname{diag}(w(\lambda, \gamma_1), w(\lambda, \gamma_2), \ldots, w(\lambda, \gamma_N)),\\
&\hat{\boldsymbol{\gamma}}(u) = (\gamma_1(u), \gamma_2(u), \ldots, \gamma_N(u))^T.
\end{aligned}$$

Finally, using known vector $\boldsymbol{\ell}^*$, the GMLS approximation $\widehat{\lambda(u)}$ for $\lambda(u)$ is

$$\widehat{\lambda(u)} = \lambda(p^*) = \mathbf{p}_\lambda^T \boldsymbol{\ell}^* = \mathbf{p}_\lambda^T (\mathbf{M}(\lambda; \gamma))^{-1} \mathbf{B}(\lambda; \gamma) \hat{\boldsymbol{\gamma}}(u), \tag{3.8}$$

where λ is an arbitrary linear functional, e.g., this functional can describe point evaluations of u, its derivatives up to order m or some local integrals. It should be noted that the weight function w in GMLS depends on functional λ and since all our functionals are finally considered as point evaluation functionals at point $\mathbf{x}$, we can choose the same $w(\mathbf{x})$ for all. The common choice in the literature is that $w(\mathbf{x}, \mathbf{x}_j)$ decreases with the distance between $\mathbf{x}_j$ and $\mathbf{x}$, in such a way that the nearer node has the greater influence. Moreover, a small domain Ω_j containing $\mathbf{x}_j$ is associated with node j such that $w(\mathbf{x}, \mathbf{x}_j)$ equals zero outside Ω_j. This choice is made to give a local character of the approximation [18,51]. The quartic spline weight function is used for all computations. This weight function is

$$w(\mathbf{x}, \mathbf{x}_j) = w(\delta_j) = \begin{cases} 1 - 6\delta_j^2 + 8\delta_j^3 - 3\delta_j^4, & \delta_j \le 1,\\ 0, & \delta_j > 1, \end{cases} \tag{3.9}$$

where $\delta_j = \frac{\|\mathbf{x} - \mathbf{x}_j\|}{R_j}$ and R_j is the radius of the support of the weight function. The size of support, R_j, of the weight function associated with node j should have enough nodes covered in the domain of definition of every sample point to ensure the regularity of matrix $\mathbf{M}$ [19]. Then the support size (the size of the influence domain) is a very important parameter in meshless methods. It is related to both accuracy of the solution, as well as the computational efficiency [52]. For the set-up of R_j, an appropriate choice can be considered as the size, which includes the least number of nodes required to avoid the singularity in the GMLS approximation. In this work, the support domain radius R_j is chosen for each node by the following procedure: It is taken $R_j = \alpha h_j$ where h_j is the distance between interior nodes when a uniform discretization is considered and the minimum distance between the neighboring points for each node $\mathbf{x}_j$ where a nonuniform discretization is given. In all computations, unless indicated otherwise, the parameter α is 2.15. It should be noted that for nonuniformly distributed nodes, the radius of the support domain is not the same for all nodes. For each grid point, if the coefficient matrix $\mathbf{M}$ is singular, the radius is further enlarged and some new points are added to the first set. The procedure is repeated until achieving a non-singular coefficient matrix.

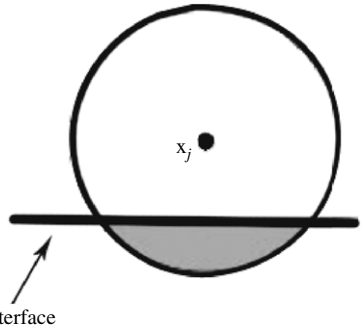

Fig. 2. Domain of influence by the visibility criterion method near an interface.

3.2. Modification of the weight function

One way to create discontinuities in the meshless approximation is the visibility criterion technique introduced by Krysl and Belytschko [23]. In this technique, a critical issue is the definition of the influence domain for a weight function. A common definition for the influence domain is that a point $\mathbf{x}$ exists in the domain of influence of a node $\mathbf{x}_j$ if the line from $\mathbf{x}$ to $\mathbf{x}_j$ has no intersect with the interface line τ. As shown in Fig. 2, the domain of influence for node $\mathbf{x}_j$ is truncated by interface τ, and the shaded area is not contained in the domain of influence for node $\mathbf{x}_j$. This truncation will be useful for the weight function of nodes that are in the vicinity of interface τ. Consider a domain with two different materials separated by the interface τ. To apply the visibility criterion technique, we first split all nodes into two sets: Λ^+ and Λ^-, where Λ^+ (Λ^-) contains all the nodes that belong exclusively to region $\bar{\Omega}^+$ ($\bar{\Omega}^-$). Also Λ_τ is a set containing the nodes lying on interface τ and Λ_b is a set containing the nodes lying on boundary $\partial\Omega$, hence $\Lambda_b \subset \Lambda^+$ and $\Lambda_\tau = \Lambda^+ \cap \Lambda^-$. In practice, two sets of nodes are assigned on both the $+$ side and the $-$ side of the material interface τ at the same location, but with different material properties. For the modification of the weight function, we will have the following procedure:

$$w^{\pm}(\mathbf{x}_i, \mathbf{x}_j) = \begin{cases} w(\mathbf{x}_i, \mathbf{x}_j), & \mathbf{x}_i, \mathbf{x}_j \in \Lambda^{\pm}, \\ 0, & \text{otherwise.} \end{cases} \tag{3.10}$$

Using the modification of the weight function, the approximation $\widehat{\lambda}(u(\mathbf{x}))$ to the $\lambda(u(\mathbf{x}))$ is then given by

$$\widehat{\lambda}(u(\mathbf{x})) = \widehat{\lambda}^{\pm}(u(\mathbf{x})), \quad \mathbf{x} \in \bar{\Omega}^{\pm}, \tag{3.11}$$

where

$$\widehat{\lambda}^{\pm}(u(\mathbf{x})) = \sum_{j=1}^{N_{\Lambda^{\pm}}} a_j(\lambda^{\pm}) u(\mathbf{x}_j^{\pm}). \tag{3.12}$$

It should be noted that in this technique, nodes from one region are not required to influence the other, even if theoretically their influence domains could be extended over there [38]. Therefore, the support domain of a point from region $\Omega^+ \cup \partial\Omega$ contains only nodes from Λ^+. Similarly, the support domain of a point from region Ω^- contains only nodes from Λ^-. Finally, the support domain of a point on τ contains nodes from Λ^+ and Λ^-. One can easily see, the high order continuity is kept within each subregion, but not across their interface [40,42].

3.3. Derivation of the discretized equations

Meshless methods write everything entirely in terms of the scattered nodes $\{\mathbf{x}_1, \ldots, \mathbf{x}_{N_\Lambda}\}$. In this work, the nodes are located in the spatial domain $\Omega^{\pm}$ and its boundary $\partial\Omega$ and interface τ. The nodes inside $\Omega^{\pm}$ are called the interior nodes, and those located exactly at $\partial\Omega$ are the boundary nodes and a double layer of nodes exists along the interface τ. The nodes lying at the interface are doubled, i.e. each interface node is actually considered equivalent to two nodes, one belonging to region Ω^+ and the other to region Ω^-. After the nodal distribution is set up, one proceeds to evaluate the local weak forms. We use the Heaviside step function as a test function over a local domain Ω_q.

To apply the DMLPG method, for any discretization of differential equation, boundary condition and interface jump condition, we first consider appropriate functionals $\lambda_i(u)$, where $\lambda_i(u) = b_i,\ i = 1, 2, \ldots, N_\Lambda$. Then, by taking the appropriate functional corresponding to each point and using the GMLS approximation for these functionals, we obtain the linear system $\mathbf{Au} = \mathbf{b}$ where each node corresponds to a row of the matrix $\mathbf{A}$. It should be noted that for each point of interface, two components of the unknown vector $\mathbf{u}$ and two rows of the matrix $\mathbf{A}$ are considered. In the DMLPG method by employing GMLS approximation, the goal is just to find good estimates for the target functionals λ_i in terms of the values at nodes, to set up the matrix $\mathbf{A}$.

Consider $\mathbf{x}_i \in \Lambda^s; s = \pm$ is an interior node with support $\Omega_q^i (\Omega_q^i \subset \Omega^s; \partial\Omega_q^i = L_q^i)$. The functional $\lambda_i^s(u)$ and right vector b_i corresponding to this node will be

$$\lambda_i^s(u) := -\int_{L_q^i} \beta^s \frac{\partial u^s}{\partial \mathbf{n}} d\Gamma + \int_{\Omega_q^i} \kappa^s u^s d\Omega, \tag{3.13}$$

$$b_i := \int_{\Omega_q^i} f^s d\Omega. \tag{3.14}$$

Using (3.11)–(3.12), the approximation of the functional (3.13) will be as follows

$$\widehat{\lambda_i^s}(u) = \sum_{j=1}^{N_{\Lambda^s}} a_j(\lambda_i^s) u(\mathbf{x}_j^s) = \mathbf{p}_{\lambda_i^s}^T \{\mathbf{M}^s\}^{-1} \mathbf{B}^s \mathbf{u}^s, \tag{3.15}$$

where

$$\mathbf{p}_{\lambda_i^s} = (\rho_1^s, \rho_2^s, \ldots, \rho_Q^s)^T; \qquad \rho_k^s = -\int_{L_q^i} \beta^s \frac{\partial p_k}{\partial \mathbf{n}} d\Gamma + \int_{\Omega_q^i} \kappa^s p_k d\Omega,$$

$$\mathbf{M}^s = \mathbf{B}^s \mathbf{P}^{s^T}; \qquad \mathbf{B}^s = \mathbf{P}^s \mathbf{W}^s; \qquad \mathbf{u}^s = (u(\mathbf{x}_1^s), u(\mathbf{x}_2^s), \ldots, u(\mathbf{x}_{N_{\Lambda^s}}^s))^T,$$

$$\mathbf{P}^s = (\mathbf{p}(\mathbf{x}_1^s), \ldots, \mathbf{p}(\mathbf{x}_{N_{\Lambda^s}}^s)); \qquad \mathbf{p}(\mathbf{x}_k^s) = (p_1(\mathbf{x}_k^s), \ldots, p_Q(\mathbf{x}_k^s))^T;$$

$$\mathbf{W}^s = \mathrm{diag}(w(\mathbf{x}_i, \mathbf{x}_1^s), \ldots, w(\mathbf{x}_i, \mathbf{x}_{N_{\Lambda^s}}^s)).$$

As observed, in the DMLPG method, the numerical integration will be done over low-degree polynomials rather than complicated MLS shape functions in the MLPG method. Also, for every functional, the GMLS routine is called only once.

The information concerning the boundary conditions at $\partial\Omega$ comes into the problem through the boundary nodes. In the DMLPG method, Dirichlet boundary conditions are directly imposed. Then by setting $\lambda_i = \delta_{\mathbf{x}_i}$, for the Dirichlet boundary node $\mathbf{x}_i \in \Lambda_b$, we can obtain

$$\widehat{\lambda_i}^+(u) = \sum_{j=1}^{N_{\Lambda^+}} a_j(\delta_{\mathbf{x}_i}^+) u(\mathbf{x}_j^+) = \mathbf{p}_{\delta_{\mathbf{x}_i}^+}^T \{\mathbf{M}^+\}^{-1} \mathbf{B}^+ \mathbf{u}^+, \tag{3.16}$$

where

$$\mathbf{p}_{\delta_{\mathbf{x}_i}^+} = (p_1(\mathbf{x}_i), p_2(\mathbf{x}_i), \ldots, p_Q(\mathbf{x}_i))^T; \qquad \mathbf{M}^+ = \mathbf{B}^+ \mathbf{P}^{+^T}; \qquad \mathbf{B}^+ = \mathbf{P}^+ \mathbf{W}^+;$$

$$\mathbf{u}^+ = (u(\mathbf{x}_1^+), u(\mathbf{x}_2^+), \ldots, u(\mathbf{x}_{N_{\Lambda^+}}^+))^T,$$

$$\mathbf{P}^+ = (\mathbf{p}(\mathbf{x}_1^+), \ldots, \mathbf{p}(\mathbf{x}_{\Lambda^+}^+)); \qquad \mathbf{p}(\mathbf{x}_k^+) = (p_1(\mathbf{x}_k^+), \ldots, p_Q(\mathbf{x}_k^+))^T;$$

$$\mathbf{W}^+ = \mathrm{diag}(w(\mathbf{x}_i, \mathbf{x}_1^+), \ldots, w(\mathbf{x}_i, \mathbf{x}_{N_{\Lambda^+}}^+)).$$

Similar to the boundary conditions, the jump conditions (2.3) and (2.4) at τ are directly imposed. They are enforced at each dual interface node, one dealing with interface conditions on the function itself (2.3) and the other with conditions on the normal derivatives (2.4). Consider $\mathbf{x}_i \in \Lambda_\tau$ and the corresponding functional with this node for jump conditions (2.3)–(2.4) as follows

$$\lambda_i(u) := \lambda_i^+(u) - \lambda_i^-(u), \tag{3.17}$$

where for jump conditions (2.3) and (2.4), we have $\lambda_i^s(u) = \delta^s_{\mathbf{x}_i}(u)$ and $\lambda_i^s(u) = \beta^s \frac{\partial u^s}{\partial \mathbf{n}}$, respectively. Using (3.11)–(3.12), the approximation of the functional (3.17) will be as follows

$$\widehat{\lambda}_i(u) = \sum_{j=1}^{N_{\Lambda^+}} a_j(\lambda_i^+)u(\mathbf{x}_j^+) - \sum_{j=1}^{N_{\Lambda^-}} a_j(\lambda_i^-)u(\mathbf{x}_j^-) = \mathbf{p}^T_{\lambda_i^+}\{\mathbf{M}^+\}^{-1}\mathbf{B}^+\mathbf{u}^+ - \mathbf{p}^T_{\lambda_i^-}\{\mathbf{M}^-\}^{-1}\mathbf{B}^-\mathbf{u}^-, \tag{3.18}$$

where for the jump condition (2.3), we have $\mathbf{p}_{\lambda_i^s} = \mathbf{p}_{\delta_{\mathbf{x}_i}}$ and for the jump condition on the normal derivatives (2.4), we set $\mathbf{p}_{\lambda_i^s} = \beta^s(\frac{\partial p_1(\mathbf{x}_i)}{\partial \mathbf{n}}, \frac{\partial p_2(\mathbf{x}_i)}{\partial \mathbf{n}}, \ldots, \frac{\partial p_Q(\mathbf{x}_i)}{\partial \mathbf{n}})^T$.

Now we explain the discretization of the elasticity interface problem by the proposed method. The process of imposing the boundary condition (2.11) and jump condition (2.13) will be similar to Eqs. (2.2) and (2.3), hence, we omit their expression. In the following, we demonstrate the discretization of the local weak form at interior nodes and the imposing of jump condition on the normal derivatives.

Using Eq. (2.15), the functional $\bar{\lambda}_i^s(\bar{u})$; $s = \pm$, corresponding to the interior node $\mathbf{x}_i \in \Lambda^s$ is as follows

$$\bar{\lambda}_i^s(\bar{u}) := \int_{L_q^i} \mathbf{N}(\mathbf{x})\mathbf{D}^s\mathbf{L}\bar{u}^s d\Gamma, \tag{3.19}$$

where

$$\bar{\lambda}_i^s(\bar{u}) = \begin{bmatrix} \lambda_i^s(u_1) \\ \lambda_i^s(u_2) \end{bmatrix}, \qquad \mathbf{N}(\mathbf{x}) = \begin{bmatrix} n_1(\mathbf{x}) & 0 & n_2(\mathbf{x}) \\ 0 & n_2(\mathbf{x}) & n_1(\mathbf{x}) \end{bmatrix}, \qquad \mathbf{D}^s = \begin{bmatrix} \lambda^s + 2\mu^s & \lambda^s & 0 \\ \lambda^s & \lambda^s + 2\mu^s & 0 \\ 0 & 0 & \mu^s \end{bmatrix},$$

$$\mathbf{L} = \begin{bmatrix} \frac{\partial}{\partial x} & 0 \\ 0 & \frac{\partial}{\partial y} \\ \frac{\partial}{\partial y} & \frac{\partial}{\partial x} \end{bmatrix}, \qquad \bar{u}^s = \begin{bmatrix} u_1^s \\ u_2^s \end{bmatrix}.$$

Using (3.11)–(3.12), the approximation of the functional (3.19) will be as follows

$$\widehat{\bar{\lambda}}_i^s(\bar{u}) = \bar{\mathbf{P}}_{\bar{\lambda}_i^s} \otimes \{\{\mathbf{M}^s\}^{-1}\mathbf{B}^s\}\bar{\mathbf{u}}^s, \tag{3.20}$$

where $\bar{\mathbf{P}}_{\bar{\lambda}_i^s} = \int_{L_q^i}\{\mathbf{N}(\mathbf{x})\mathbf{D}^s\mathbf{L}\} \otimes \mathbf{p}^s d\Gamma$, $\mathbf{p}^s = (p_1^s, p_2^s, \ldots, p_Q^s)$. Similar to Eq. (3.15), for Eq. (3.20) we observe that integration over the MLS shape functions is avoided and, is replaced by the integration over polynomials.

To apply the jump condition (2.14), at the arbitrary interface node $x_i \in \Lambda_\tau$, the appropriate functional will be:

$$\bar{\lambda}_i(\bar{u}) := \mathbf{N}(\mathbf{x}_i)\{\mathbf{D}^+\mathbf{L}\bar{u}^+(\mathbf{x}_i) - \mathbf{D}^-\mathbf{L}\bar{u}^-(\mathbf{x}_i)\}. \tag{3.21}$$

Using (3.11)–(3.12), the approximation of the functional (3.21) will be as follows

$$\widehat{\bar{\lambda}}_i(\bar{u})|_{\mathbf{x}_i} = \widehat{\bar{\lambda}}_i^+(\bar{u})|_{\mathbf{x}_i} - \widehat{\bar{\lambda}}_i^-(\bar{u})|_{\mathbf{x}_i}, \tag{3.22}$$

where

$$\widehat{\bar{\lambda}}_i^s(\bar{u})|_{\mathbf{x}_i} = \bar{\mathbf{P}}_{\bar{\lambda}_i^s}|_{\mathbf{x}_i} \otimes \{\{\mathbf{M}^s\}^{-1}\mathbf{B}^s\}\bar{\mathbf{u}}^s, \quad \bar{\mathbf{P}}_{\bar{\lambda}_i^s} = \{\mathbf{N}(\mathbf{x})\mathbf{D}^s\mathbf{L}\} \otimes \mathbf{p}^s.$$

As seen from Eqs. (3.15), (3.18), (3.20) and (3.22), derivative and integration of MLS shape functions are not needed in the construction of the stiffness matrix. Due to the rapidly increasing of MLPG running time by gradually increase of nodes, the DMLPG method can be efficient for the complex problems that require the refinement strategy. It should be noted that, practically, the difference between the two methods (DMLPG and MLPG) is in calculating the entries of the stiffness matrix. In the next section, the computational cost of production of the stiffness matrix will be compared.

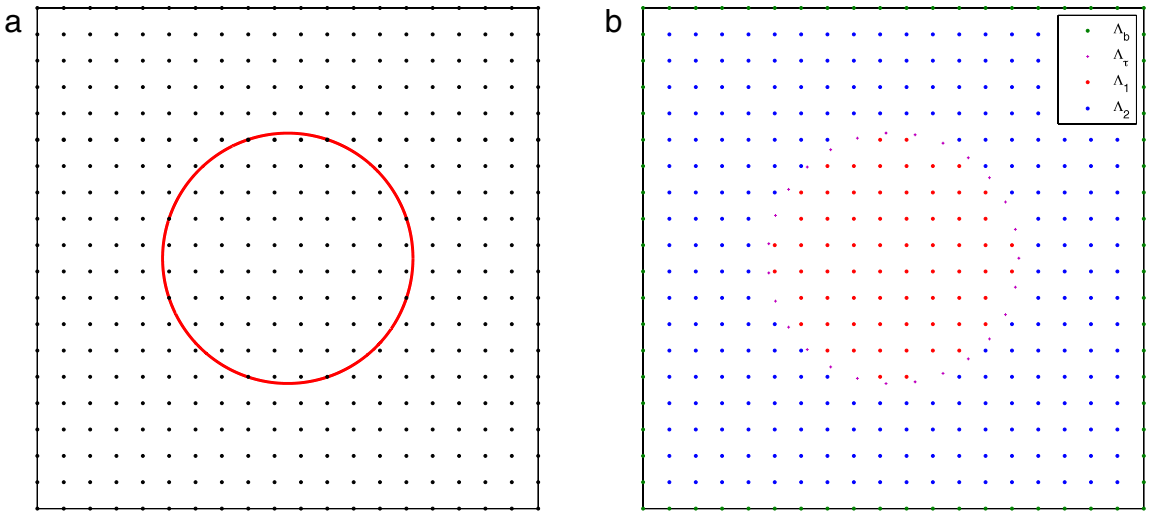

Fig. 3. (a) Regular grid containing the plate. (b) Λ_b, Λ_τ, Λ_1, Λ_2 refer to the nodal points of global boundary $\partial\Omega$, interface τ, interior nodes of Ω^- and interior nodes of Ω^+, respectively.

4. Numerical experiments

We investigate the efficiency and accuracy of the proposed method for the interface problems such as Poisson, linearized Poisson–Boltzmann and elasticity problems. Numerical results are compared with classical MLPG in terms of both numerical accuracy and computational efficiency. As previously mentioned, the difference between MLPG and DMLPG methods is in construction of the stiffness matrix. We compare the CPU time of the generated stiffness matrix for both methods. For the first three test examples, the computational domain Ω is the rectangle $(x, y) \in [-1, 1] \times [-1, 1]$ and the interface τ is represented by a circle with center at the origin and radius $r_0 = 0.5$. The interface τ separates the domain $\bar{\Omega}$ into two subregions $\bar{\Omega}^+$ and $\bar{\Omega}^-$ with $\bar{\Omega}^- = \{(x, y) : x^2 + y^2 \leq 1/4\}$. Also, the solution is approximated over uniformly distributed mesh points. In order to construct a nodal distribution for the studied geometry, we use the following strategy. Initially, the global domain Ω and the interface τ are considered. Then, a regular grid containing the geometry is generated (see Fig. 3(a)). After that, the nodes on or very close neighborhood of interface τ are omitted. Finally, the rest of grids is confined into the $\partial\Omega \cup \Omega^+$ and Ω^- and a uniform nodal distribution is considered for the interface τ with the number of points N_{Λ_τ} (see Fig. 3(b)). However, the primary interest of the meshless methods is that they should work on arbitrary curved interface and on irregular clouds of points. The final test is devoted to the ability of the proposed method to deal with the complicated interface with two different nodal distributions (regular and irregular). The distribution of points for the considered complex interface problem is shown in Fig. 4. It should be noted that the distributed strategy is the same as the previous examples. In all tables, N_{Λ^-} and N_{Λ^+} denote the number of points in the subregions $\bar{\Omega}^-$ and $\bar{\Omega}^+$, respectively. Integration of local weak forms is carry out numerically by a Gaussian quadrature [53]. To compare the proposed method with MLPG, the 12×12 quadrature points are used to numerically evaluate integrals over each subdomain, and 15 points are used on each section of L_q. To have greater stability, we use the shifted and scaled polynomials as basis functions in GMLS [44] where the quadratic polynomial basis is considered. It should be noted that the size of the local subdomain r_i for each node is taken $r_i = \gamma h_i$ where h_i is being the minimum distance between the neighboring points in the interior domain. In all computations, unless indicated otherwise, the parameter γ is 0.8. To avoid the intersection between the test domain Ω_q^i associated to an interior node $\mathbf{x}_i$ and the interface boundary τ, the test domain radius r_i is chosen as $r_i < d_i$ where d_i is the distance between the interior node $\mathbf{x}_i$ and τ. This procedure ensures that if the interior node is too close to the interface boundary, the associated test domain is chosen so that it just touches τ.

Example 1. In the first example, we study the Poisson interface problem with three different jump conditions. To compare the accuracy of both schemes (MLPG and DMLPG), we consider the different parameters α and γ for the trial and test domains, respectively.

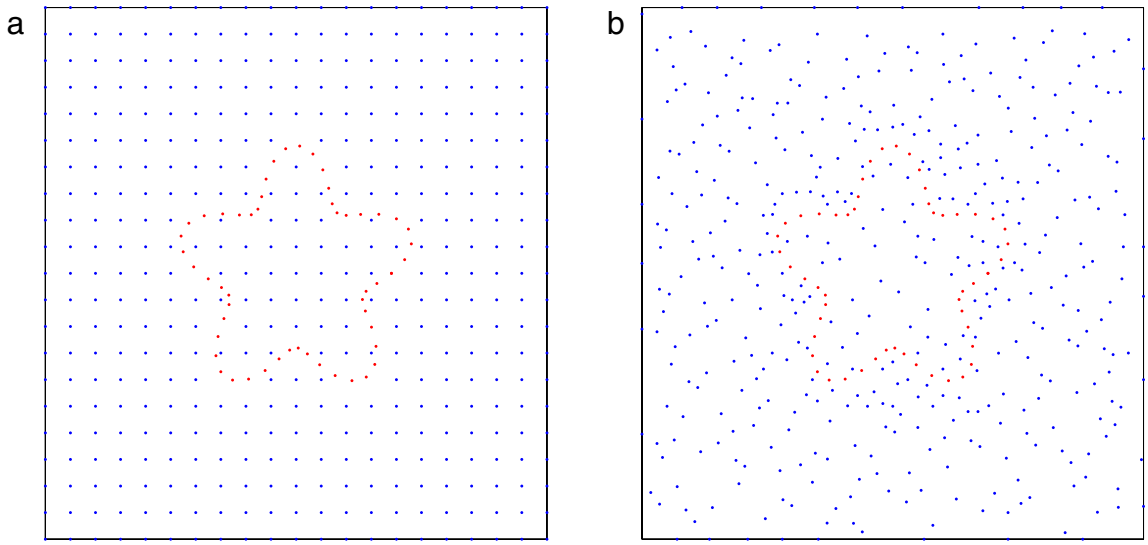

Fig. 4. Distribution of nodes in Example 4: (a) regular distribution and (b) irregular distribution.

Table 1
The values of L_2-norm errors with DMLPG method for Case I in Example 1.

$(N_{\Lambda^-}, N_{\Lambda^+})$	(31, 93)	(95, 351)	(320, 1312)	(693, 2937)
$\beta^- = 1, \beta^+ = 2$	3.20e−2	6.32e−3	2.49e−3	9.22e−4
$\beta^- = 1, \beta^+ = 10$	2.09e−2	5.71e−3	1.80e−3	6.71e−4
$\beta^- = 1, \beta^+ = 1000$	1.76e−2	4.11e−3	1.19e−3	6.15e−4

Case I. (Homogeneous jump in the solution and its flux across the interface):

Let $\nabla \cdot (\beta \nabla u) = 9\sqrt{x^2 + y^2}$ with the exact solution [54]

$$u(x, y) = \begin{cases} \dfrac{(x^2 + y^2)^{3/2}}{\beta^-}, & \text{on } \Omega^-, \\ \dfrac{(x^2 + y^2)^{3/2}}{\beta^+} + \dfrac{1}{8}\left(\dfrac{1}{\beta^-} - \dfrac{1}{\beta^+}\right), & \text{on } \Omega^+. \end{cases}$$

It is easy to check that in this case the solution and its normal derivative of the solution are continuous ($[u]_\tau = 0$, $[\beta \frac{\partial u}{\partial n}]_\tau = 0$). In this case, we investigate the problem with large jumps in the coefficients at the interface. To validate the asymptotic behavior of the approximation error with the increasing of the jump in β, a series of β^+ are chosen for this case. The error of the numerical solution in terms of the L_2-norm is collected in Table 1 for $\beta^- = 1$ and $\beta^+ = 2, 10, 1000$.

Also, in Fig. 5, MLPG and DMLPG are compared in accuracy and CPU time with $\beta^- = 1$ and $\beta^+ = 100$.

Case II. (Non-homogeneous jump in the flux across the interface):

Consider $\nabla^2 u = 0$ with the jump conditions $[u]_\tau = 0$ and $[u_n]_\tau = 2$. This can be considered as a problem where there is a singular source term along the interface, and the exact solution is given as [55]

$$u(x, y) = \begin{cases} 1, & \text{on } \Omega^-, \\ 1 + \log(2\sqrt{x^2 + y^2}), & \text{on } \Omega^+. \end{cases}$$

The errors of numerical results by the DMLPG method are given in Table 2. Fig. 6 shows a comparison between MLPG and DMLPG methods for accuracy and CPU time.

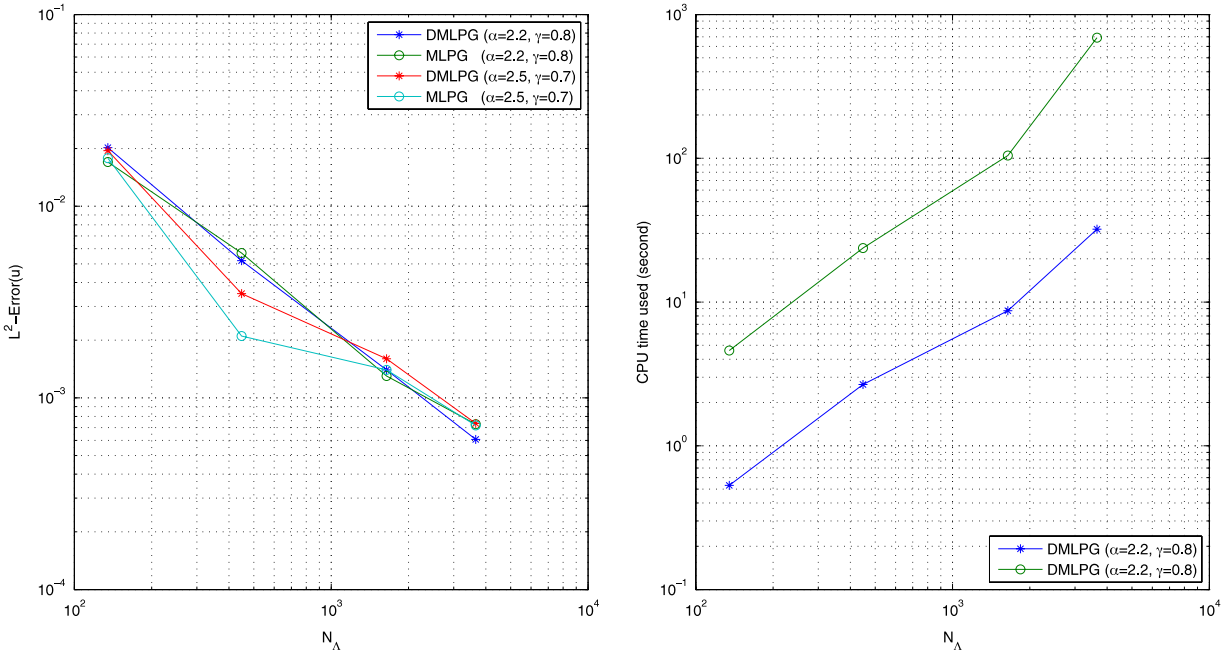

Fig. 5. Comparison between MLPG and DMLPG methods for Case I in Example 1 with $N_\Lambda = \{135, 448, 1642, 3652\}$.

Table 2
The values of L_2-norm errors with DMLPG method for Case II in Example 1.

$(N_{\Lambda^-}, N_{\Lambda^+})$	(31, 93)	(95, 351)	(320, 1312)	(693, 2937)
	1.25e−2	2.60e−3	6.54e−4	3.75e−4

Case III. (Non-homogeneous jump in the solution and its flux across the interface):
Consider $\nabla \cdot (\beta \nabla u) = f$, where the analytical solution to the equation, the coefficient β, and the inhomogeneous term of the equation are given as follow [56]

$$u(x,y) = \begin{cases} x^2 + y^2 - 1, & \Omega^-, \\ \dfrac{1}{4}\left(1 - \dfrac{1}{8b} - \dfrac{1}{b}\right) + \left(\dfrac{(x^2+y^2)^2}{2} + x^2 + y^2\right) \Big/ b, & \Omega^+, \end{cases}$$

$$\beta(x,y) = \begin{cases} 2, & \Omega^-, \\ b, & \Omega^+, \end{cases}$$

$$f(x,y) = \begin{cases} 8, & \Omega^-, \\ 8(x^2+y^2) + 4, & \Omega^+. \end{cases}$$

By choosing $b = 10$, it can be checked that jump conditions are $[u]_\tau = 1$ and $[\beta u_n]_\tau = -0.75$. Table 3 reports refinement of the proposed method for this problem. Fig. 7 demonstrates the comparison of MLPG and DMLPG techniques for accuracy and computational cost.

For all three cases we observe that the numerical errors are small. Hence, the proposed method gives a good accuracy for each type of jump condition. Figs. 5–7 show that difference of errors is small in both schemes DMLPG and MLPG, but the DMLPG method uses less computational time.

Example 2 (*Linearized Poisson–Boltzmann Problem*)**.** In this example, we study the behavior of the proposed method for the linearized Poisson–Boltzmann equation with different dielectric constants. Consider

$$\nabla \cdot (\beta \nabla u(x,y)) + k^2(x,y)u(x,y) = f(x,y),$$

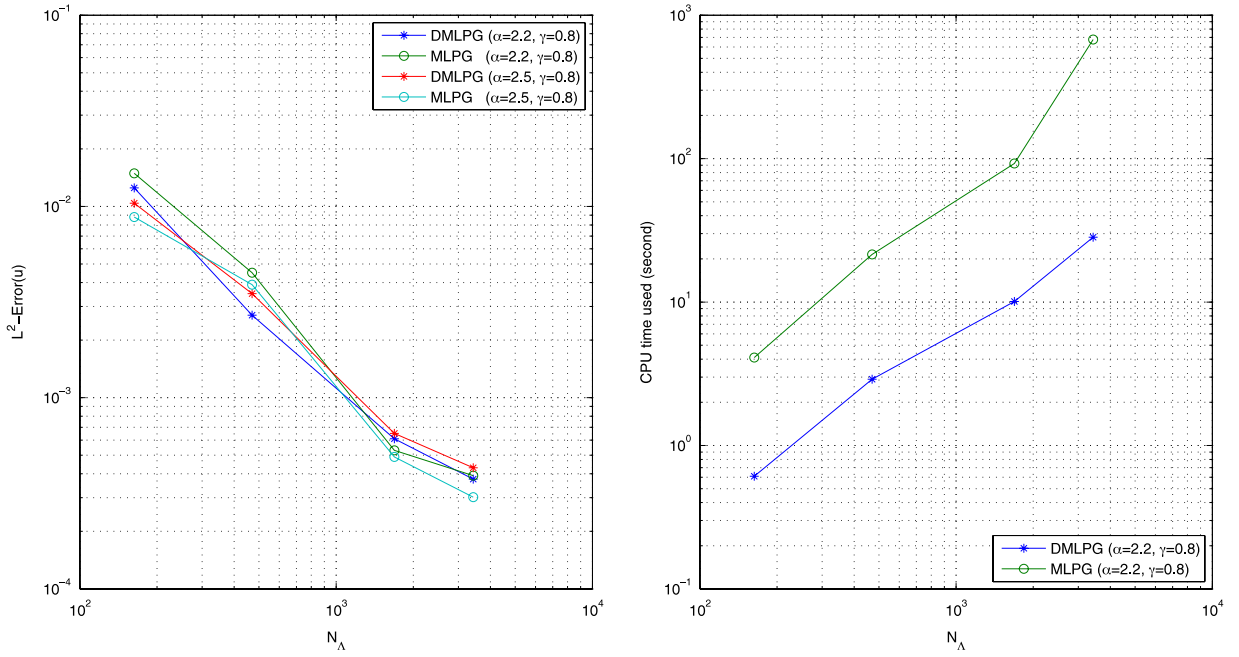

Fig. 6. Comparison between MLPG and DMLPG methods for Case II in Example 1 with $N_\Lambda = \{163, 470, 1688, 3428\}$.

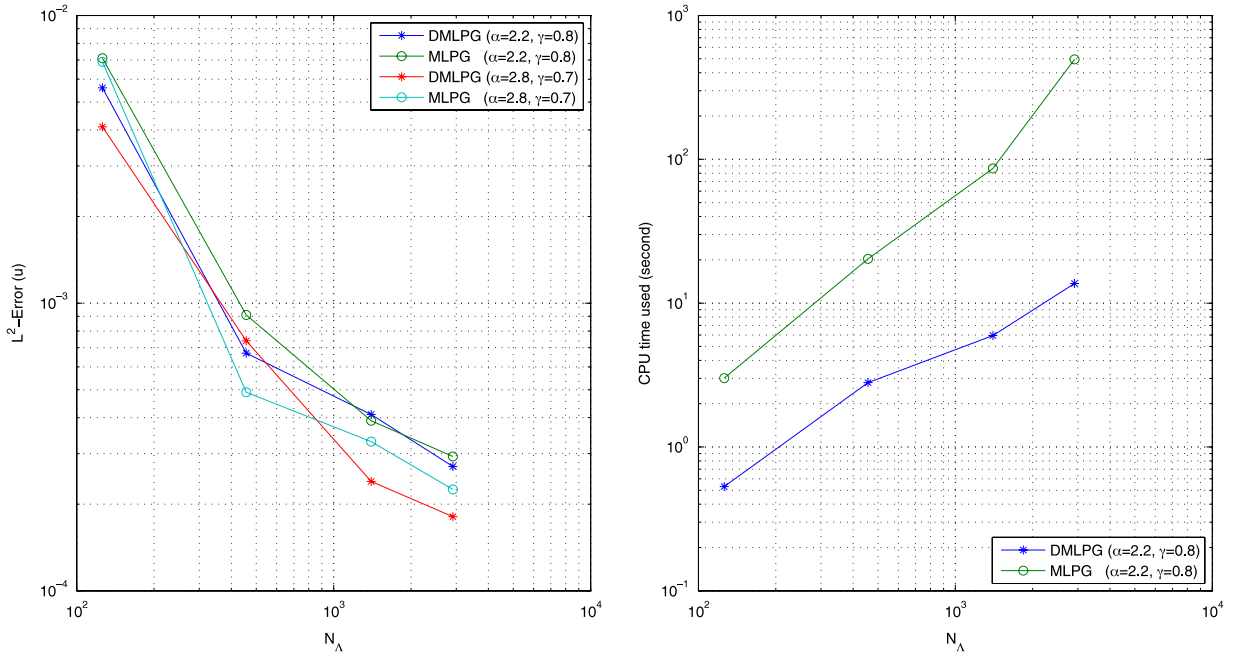

Fig. 7. Comparison between MLPG and DMLPG methods for Case III in Example 1 with $N_\Lambda = \{126, 457, 1400, 2910\}$.

Table 3
The values of L_2-norm errors with DMLPG method for Case III in Example 1.

$(N_{\Lambda^-}, N_{\Lambda^+})$	(31, 93)	(95, 351)	(320, 1312)	(693, 2937)
	5.61e−3	7.30e−4	2.44e−4	9.17e−5

Table 4
The values of L_2-norm errors for displacement u with DMLPG method in Example 2.

$(N_{\Lambda^-}, N_{\Lambda^+})$	(31, 93)	(95, 351)	(320, 1312)	(693, 2937)
$\kappa = 1$	8.11e−3	2.03e−3	5.74e−4	3.70e−4
$\kappa = 5$	1.82e−1	4.17e−2	9.41e−3	5.20e−3
$\kappa = 10$	8.61e−1	5.35e−1	1.21e−1	9.12e−2

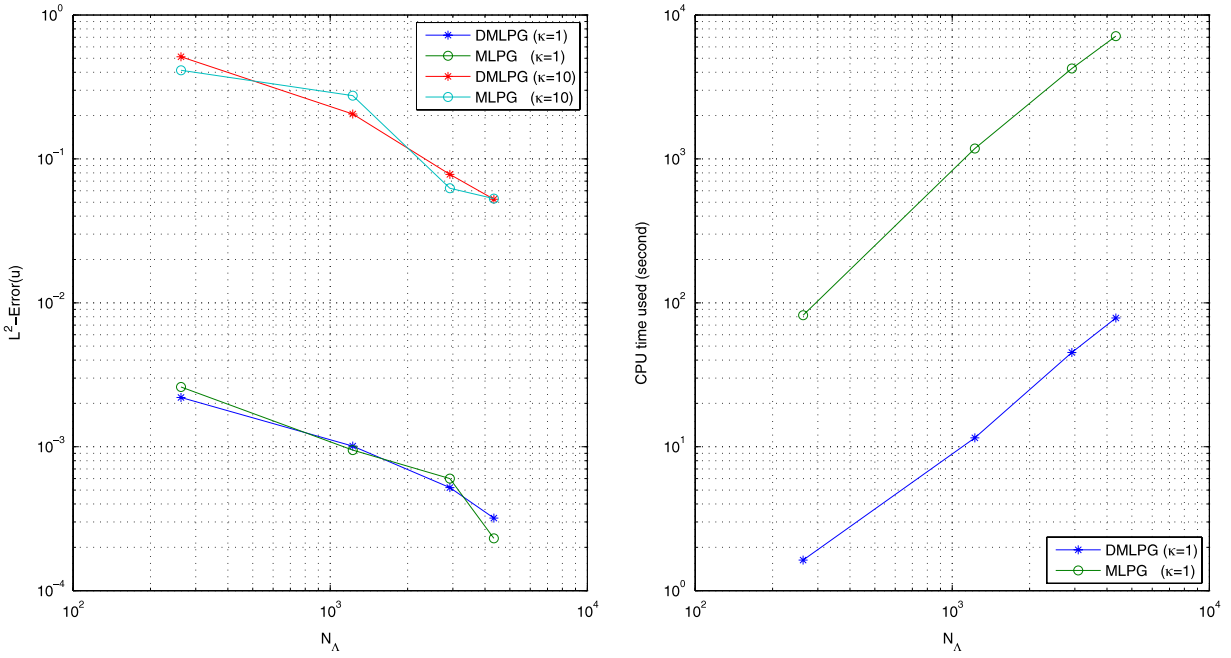

Fig. 8. Comparison between MLPG and DMLPG methods in Example 2 with $N_\Lambda = \{263, 1224, 2920, 4330\}$.

where the discontinuous coefficients β and σ are

$$\beta(x, y) = \begin{cases} 10, & \Omega^-, \\ 1, & \Omega^+, \end{cases}$$

$$\sigma(x, y) = \begin{cases} 1, & \Omega^-, \\ \sqrt{10}, & \Omega^+, \end{cases}$$

and $k(x, y) = \kappa\sigma(x, y)$ is the dielectric function describing macroscopically the properties of the propagation wave. The analytical solution to this equation is as follows [56]

$$u(x, y) = \begin{cases} x^2 + y^2, & \Omega^-, \\ \sin(\kappa x)\cos(\kappa y), & \Omega^+. \end{cases}$$

As κ can be tuned to produce solutions of desired frequency, three different frequencies with $\kappa = 1, 5$ and 10 are considered in Table 4. Also, the comparison of DMLPG and MLPG methods is provided for two frequencies with $\kappa = 1$ and 10. The comparison is plotted in Fig. 8. It is observed that the low frequency solution can be well approximated by both schemes but we notice the errors increase by increasing frequency (see Table 4 for DMLPG method and Fig. 8 for both MLPG and DMLPG techniques). However, the numerical results are improved by increasing the number of points.

Fig. 8 shows that the accuracy of DMLPG and MLPG techniques can be the same but the computational cost of the DMLPG method decreases significantly in comparison with the MLPG method.

Table 5
The relative errors in the L_2-norm with DMLPG method in Example 3.

$(N_{\Lambda^-}, N_{\Lambda^+})$		(31, 93)	(95, 351)	(320, 1312)	(693, 2937)
Plane strain	Error (displacement)	5.73e−2	1.92e−2	3.04e−3	1.95e−3
	Error (strain)	5.12e−1	1.98e−1	9.13e−2	6.15e−2
Plane stress	Error (displacement)	3.35e−2	9.58e−3	2.17e−3	1.58e−3
	Error (strain)	4.85e−1	1.95e−1	8.95e−2	4.91e−2

$(E^-, E^+) = (1, 1000)$, $(\nu^-, \nu^+) = (0.25, 0.3)$.

Table 6
The relative errors in the L_2-norm with DMLPG method in Example 3.

$(N_{\Lambda^-}, N_{\Lambda^+})$		(31, 93)	(95, 351)	(320, 1312)	(693, 2937)
Plane strain	Error (displacement)	1.55e−2	5.92e−3	1.04e−3	9.46e−4
	Error (strain)	4.91e−1	1.81e−1	8.8e−2	5.17e−2
Plane stress	Error (displacement)	1.03e−2	2.05e−3	1.25e−3	7.22e−4
	Error (strain)	4.71e−1	1.91e−1	8.73e−2	4.12e−2

$(E^-, E^+) = (1, 10)$, $(\nu^-, \nu^+) = (0.1, 0.4)$.

Example 3 (*Elastostatic Problem*)**.** In this example, the elasticity problem in a square plate with circular inclusion is presented, where the displacement field is continuous with discontinuous strains. The inside and outside of the interface, the material parameters are (E^-, ν^-) and (E^+, ν^+), respectively. At any point, the displacement vector can be written $\mathbf{u} = (u_r, u_\theta)$, where u_r is the radial component of the displacement and u_θ is the circumferential component. The exact displacement solution of this problem is given by [48]

$$u_r(r,\theta) = \begin{cases} \left[\left(1 - \dfrac{4}{a^2}\right)\alpha + \dfrac{4}{a^2}\right] r, & \Omega^-, \\ \left(r - \dfrac{4}{r}\right)\alpha + \dfrac{4}{r}, & \Omega^+, \end{cases}$$

$$u_\theta(r,\theta) = 0,$$

and the radial (ϵ_{rr}) and hoop ($\epsilon_{\theta\theta}$) strains are given by:

$$\epsilon_{rr}(r,\theta) = \begin{cases} \left(1 - \dfrac{4}{a^2}\right)\alpha + \dfrac{4}{a^2}, & \Omega^-, \\ \left(1 + \dfrac{4}{r^2}\right)\alpha - \dfrac{4}{r^2}, & \Omega^+, \end{cases}$$

$$\epsilon_{\theta\theta}(r,\theta) = \begin{cases} \left(1 - \dfrac{4}{a^2}\right)\alpha + \dfrac{4}{a^2}, & \Omega^-, \\ \left(1 - \dfrac{4}{r^2}\right)\alpha + \dfrac{4}{r^2}, & \Omega^+, \end{cases}$$

where $\alpha = \frac{4(\lambda^- + \mu^- + \mu^+)}{(\lambda^+ + \mu^+)a^2 + (\lambda^- + \mu^-)(4 - a^2) + 4\mu^+}$.

In the following, the solution of the elasticity interface problem in both plane strain state and plane stress state is studied. We compute the results of the relative errors in the L_2-norm of displacements and strains by varying the number of particles. Tables 5 and 6 show the convergence with mesh refinement of the proposed method for two different material parameters $(E^-, E^+) = (1, 1000)$, $(\nu^-, \nu^+) = (0.25, 0.3)$ and $(E^-, E^+) = (1, 10)$, $(\nu^-, \nu^+) = (0.1, 0.4)$, respectively. Compared with the analytical solutions, good agreements are obtained for both states, i.e., plane strain and plane stress. To compare with conventional MLPG, the relative errors in the L_2-norm for numerical solutions of displacements and strains and also CPU time for the generation of stiffness matrix are reported in Fig. 9 for the plane strain state with $(E^-, E^+) = (1, 1000)$, $(\nu^-, \nu^+) = (0.1, 0.4)$. This figure shows that the accuracy of two techniques is good but DMLPG method uses less computational time. Also, the numerical solution of strains,

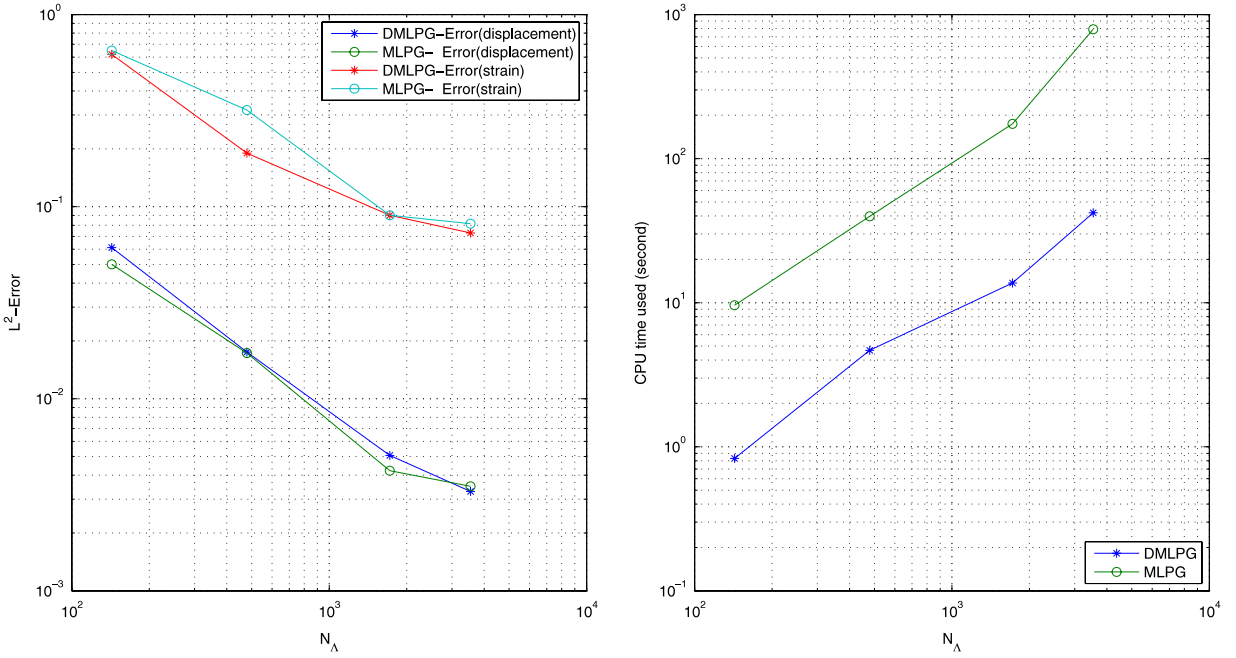

Fig. 9. Comparison between MLPG and DMLPG methods in Example 3 with $N_\Lambda = \{143, 479, 1720, 3540\}$.

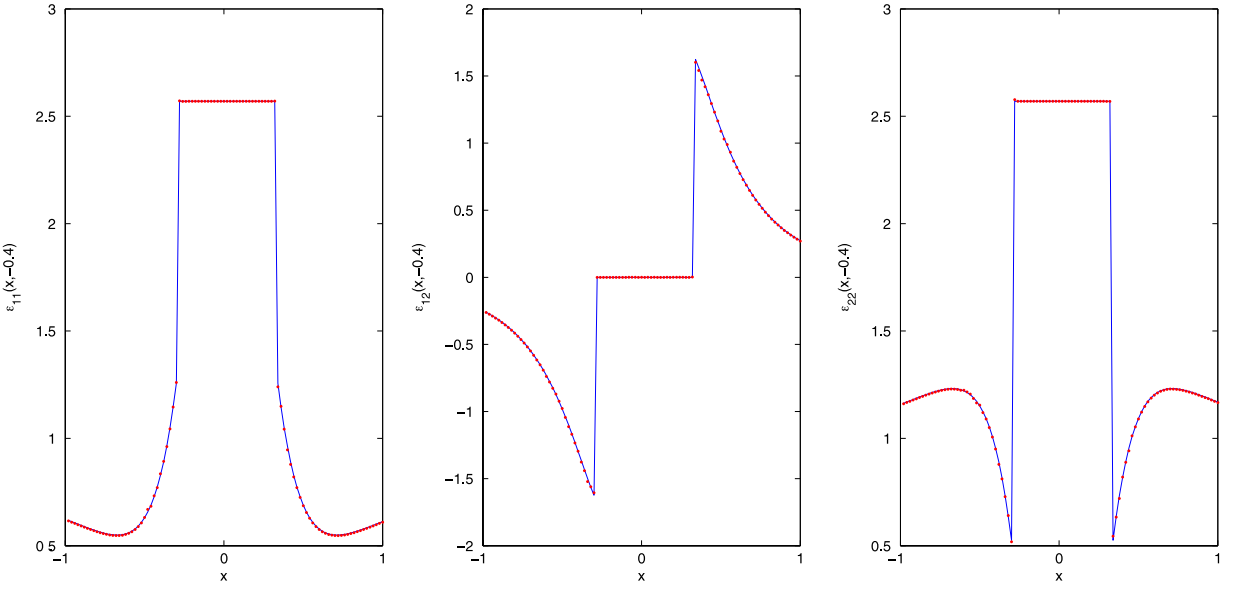

Fig. 10. Comparison of exact and numerical solutions of strains $(\epsilon_{11}(x, -0.4), \epsilon_{12}(x, -0.4), \epsilon_{22}(x, -0.4))$ in Example 3.

$\epsilon_{11}(x, -0.4), \epsilon_{12}(x, -0.4), \epsilon_{22}(x, -0.4)$, is compared with the analytical solution by using the proposed method in Fig. 10. In this test, we considered the plane stress condition with $(E^-, E^+) = (1, 10)$, $(\nu^-, \nu^+) = (0.1, 0.4)$ and 3630 points.

Example 4 (*Complex Interface Problem*)**.** As a testing of the proposed method for more complex geometry, we consider the jump problem $\nabla(\beta\nabla u) = f$, with the interface geometry τ defined by the collection of points

$$\begin{cases} X = 0.5 + (0.19 + 0.05\sin(5\theta))\cos(\theta), & \theta \in [-\pi, \pi], \\ Y = 0.5 + (0.19 + 0.05\sin(5\theta))\sin(\theta), \end{cases}$$

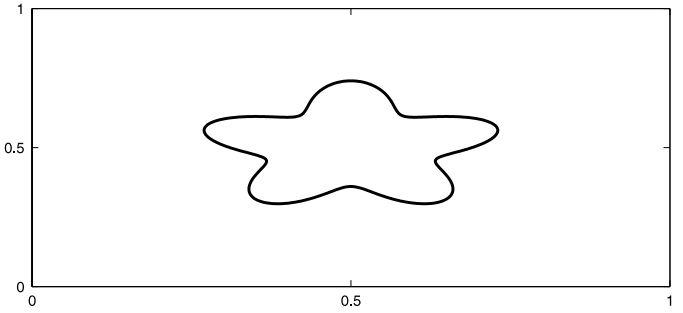

Fig. 11. The considered domain for the complex interface problem in Example 4.

Table 7
The values of L_2-norm errors displacement u with DMLPG method in Example 4.

$(N_{\Lambda^-}, N_{\Lambda^+})$	(98, 441)	(140, 663)	(270, 1560)	(376, 2396)
Regular distribution	1.24e−2	8.75e−3	4.13e−3	1.48e−3
Irregular distribution	1.12e−2	7.25e−3	5.49e−3	1.75e−3

on the rectangular domain $\Omega = [0, 1]^2$, see Fig. 11. The coefficients are chosen to be $\beta^+ = 10$ and $\beta^- = 1$. The analytical solution is given as [56]

$$u(x, y) = \begin{cases} \exp(x^2 + y^2), & \Omega^-, \\ 0.1(x^2 + y^2)^2 - 0.01 \log\left(2\sqrt{x^2 + y^2}\right), & \Omega^+. \end{cases}$$

To test the independence of the node distribution to the present method, this problem is solved with regularly and irregularly distributed nodes. In Table 7, results for both node distributions are presented and compared with exact solution. It can be seen from Table 7 that the calculation results on irregular nodes have little difference to those on uniformly distributed nodes. We refer the interested reader to [57–59] for recent works on applications of meshless procedures of various types.

5. Conclusion

Many practical problems are faced with multiple connected domains and various discontinuities in the solution or their derivatives that are known as interface problems. In this work, the direct meshless local Petrov–Galerkin (DMLPG) method with modified weight function in GMLS was successfully developed for solving Poisson, linearized Poisson–Boltzmann and planar elasticity problems with closed interface. In the DMLPG method, the approximation of test functionals associated with local weak forms is obtained using GMLS in terms of nodes without employing shape functions. So this method is considerably faster than the classical ones. To obtain accurate discontinuous solutions using the DMLPG method, we used the visibility criterion technique that is efficient for closed interfaces. The DMLPG method with visibility criterion is an attractive scheme for interface problems due to its simplicity in implementation. This technique produces appropriate approximation near the interface by cutting off the support of the weight function. To show the accuracy and efficiency of the proposed method, some test problems are investigated for the problems with homogeneous and nonhomogeneous jump conditions. The obtained results are also compared with analytical solutions and the MLPG method using the visibility criterion technique. Although, the numerical results showed that the combination of both classical MLPG and DMLPG methods with the visibility criterion technique gives accurate numerical results for the interface problems, but the mesh refinement procedure with the DMLPG method can be efficiently obtained with much less computational cost. Since the meshless methods are well-known to perform well even on irregular nodes, we observed this advantage of being able to employ arbitrary node distribution for the proposed method in solving a complex interface problem. We believe that the combination of the DMLPG technique with many enriched schemes for discontinuities can be attractive to study a wide range of interface problems.

Acknowledgments

We would like to express our thanks to three reviewers for their valuable comments and suggestions which helped to improve this paper.

References

[1] B.N.J. Persson, S. Gorb, The effect of serface roughness on the adhesion of elastic plates with application to biological systems, J. Chem. Phys. 119 (2003) 11437–11444.
[2] F. Fogolari, P. Zuccato, G. Esposito, P. Viglino, Biomolecular electrostatics with the linearized Poisson–Boltzmann equation, Biophys. J. 76 (1999) 1–16.
[3] R.J. Atkin, N. Fox, An Introduction to the Theory of Elaticity, Longman, London, 1980.
[4] H.J. Jou, P.H. Leo, J.S. Lowengrub, Microstructural evolution in inhomogeneous elastic media, J. Comput. Phys. 131 (1997) 109–148.
[5] I.S. Sokolnikoff, Mathematical Theory of Elasticity, McGraw-Hill, New York, 1956.
[6] A.P. Sutton, R.W. Balluffi, Interfaces in Crystalline Materials, in: Monographs on the Physics and Chemistry of Materials, Clarendon Press, Oxford, 1995.
[7] L. Greengard, M. Moura, On the numerical evaluation of electrostatic fields in composite materials, Acta Numer. 3 (1994) 379–410.
[8] M.A. Grinfeld, The stress driven rearrangment instability in ellastic crystals: mathematical models and physical manifestations, Nonlinear Sci. 3 (1993) 35–83.
[9] R.J. Braun, B.T. Murray, Adaptive phase-field computations of dendritic crystal growth, J. Cryst. Growth 174 (1997) 41–53.
[10] T. Fan, Mathmatical Theory of Elasticity of Quasicrystals and its Applications, Springer-Verlag, Berlin, Heidelberg, 2011.
[11] X. Yang, B. Li, Z. Li, The immersed interface method for elasticity problems with interfaces, Dyn. Contin. Discrete Impuls. Syst. Ser. A Math. Anal. 10 (2003) 783–808.
[12] T.P. Fries, T. Belytschko, The extended/generalized finite element method: an overview of the method and its applications, Internat. J. Numer. Methods Engrg. 84 (2010) 253–304.
[13] M. Dehghan, A. Shokri, Numerical solution of the nonlinear Klein–Gordon equation using radial basis functions, J. Comput. Appl. Math. 230 (2009) 400–410.
[14] M. Dehghan, A. Ghesmati, Numerical simulation of two-dimensional sine–Gordon solitons via a local weak meshless technique based on the radial point interpolation method (RPIM), Comput. Phys. Comm. 181 (2010) 772–786.
[15] M. Dehghan, A. Nikpour, Numerical solution of the system of second-order boundary value problems using the local radial basis functions based differential quadrature collocation method, Appl. Math. Model. 37 (2013) 8578–8599.
[16] R. Salehi, M. Dehghan, A moving least square reproducing polynomial meshless method, Appl. Numer. Math. 69 (2013) 34–58.
[17] A. Shokri, M. Dehghan, A Not-a–Knot meshless method using radial basis functions and predictor–corrector scheme to the numerical solution of improved Boussinesq equation, Comput. Phys. Comm. 181 (2010) 1990–2000.
[18] S.N. Atluri, T. Zhu, A new meshless local Petrov–Galerkin (MLPG) approach in computational mechanics, Comput. Mech. 22 (1998) 117–127.
[19] S.N. Atluri, S.P. Shen, The meshless local Petrov–Galerkin (MLPG) method: a simple and less-costly alternative to the finite element methods and boundary element methods, CMES Comput. Model. Eng. Sci. 3 (2002) 11–51.
[20] M. Dehghan, R. Salehi, A meshless local Petrov–Galerkin method for the time–dependent Maxwell equations, J. Comput. Appl. Math. 268 (2014) 93–110.
[21] M. Dehghan, D. Mirzaei, Meshless local Petrov–Galerkin (MLPG) method for the unsteady magnetohydrodynamic (MHD) flow through pipe with arbitrary wall conductivity, Appl. Numer. Math. 59 (2009) 1043–1058.
[22] J. Sladek, P. Stanak, Z.D. Han, V. Sladek, S.N. Atluri, Application of the MLPG method in engineering and sciences: a Review, CMES Comput. Model. Eng. Sci. 92 (2013) 423–475.
[23] P. Krysl, T. Belytschko, Element-free Galerkin method: convergence of the continuous and discontinuous shape functions, Comput. Methods Appl. Mech. Engrg. 148 (1997) 257–277.
[24] T. Belytschko, M. Fleming, Smoothing, enrichment and contact in the element-free Galerkin method, Comput. Struct. 71 (1999) 173–195.
[25] R.C. Batra, M. Porfiri, D. Spinello, Treatment of material discontinuity in two meshless local Petrov–Galerkin (MLPG) formulations of axisymmetric transient heat conduction, Internat. J. Numer. Methods Engrg. 61 (2004) 2461–2479.
[26] T. Belytschko, Y. Krongauz, D. Organ, M. Fleming, P. Krysl, Meshless methods: an overview and recent developments, Comput. Methods Appl. Mech. Engrg. 139 (1996) 3–47.
[27] L.W. Cordes, B. Moran, Treatment of material discontinuity in the element-free Galerkin method, Comput. Methods Appl. Mech. Engrg. 139 (1996) 75–89.
[28] M. Duflot, H. Nguyen-Dang, A meshless method with enriched weight functions for fatigue crack growth, Internat. J. Numer. Methods Engrg. 59 (2004) 1945–1961.
[29] M. Fleming, Y.A. Chu, B. Moran, T. Belytschko, Enriched element-free Galerkin methods for crack tip fields, Internat. J. Numer. Methods Engrg. 40 (1997) 1483–1504.
[30] Y. Krongauz, T. Belytschko, EFG approximation with discontinuous derivatives, Internat. J. Numer. Methods Engrg. 41 (1998) 1215–1233.
[31] Q. Li, S. Shen, Z.D. Han, S.N. Atluri, Application of meshless local Petrov–Galerkin (MLPG) to problems with singularities, and material discontinuities, in 3-D elasticity, CMES Comput. Model. Eng. Sci. 4 (2003) 571–585.
[32] S. Masuda, H. Noguchi, Analysis of structure with material interface by meshfree method, CMES Comput. Model. Eng. Sci. 11 (2006) 131–144.

[33] V.P. Nguyen, T. Rabczuk, S. Bordas, M. Duflot, Meshless methods: a review and computer implementation aspects, Math. Comput. Simul. 79 (2008) 763–813.
[34] W.L. Nicomedes, R.C. Mesquita, F.J.S. Moreira, 2-D Scattering integral field equation solution through an IMLS meshless-based approach, IEEE Trans. Magn. 46 (2010) 2783–2786.
[35] H. Pathak, A. Singh, I.V. Singh, Fatigue crack growth simulations of homogeneous and bi-material interfacial cracks using element free Galerkin method, Appl. Math. Model. (2014). http://dx.doi.org/10.1016/j.apm.2013.11.030.
[36] D. Wang, J.S. Chen, L. Sun, Homogenization of magnetostrictive particle-filled elastomers using an interface-enriched reproducing kernel particle method, Finite Elem. Anal. Des. 39 (2003) 765–782.
[37] D. Wang, Y. Sun, L. Li, A discontinuous Galerkin meshfree modeling of material interface, CMES Comput. Model. Eng. Sci. 45 (2009) 57–82.
[38] W.L. Nicomedes, R.C. Mesquita, F.J.S. Moreira, The meshless local Petrov–Galerkin method in two-dimensional electromagnetic wave analysis, IEEE Trans. Antennas and Propagation 60 (2012) 1957–1968.
[39] W.L. Nicomedes, R.C. Mesquita, F.J.S. Moreira, A meshless local Petrov–Galerkin method for three-dimensional scalar problems, IEEE Trans. Magn. 47 (2011) 1214–1217.
[40] J. Sladek, V. Sladek, S. Krahulec, C.H. Zhang, Interface crack problems in anisotropic solids analyzed by the MLPG, CMES Comput. Model. Eng. Sci. 54 (2009) 223–252.
[41] J. Sladek, V. Sladek, S. Krahulec, M. Wunsche, C.H. Zhang, MLPG analysis of layered composites with piezoelectric and piezomagnetic phases, CMC Comput. Mater. Continua 29 (2012) 75–102.
[42] J. Sladek, V. Sladek, M. Wunsche, C.H. Zhang, Analysis of an interface crack between two dissimilar piezoelectric solids, Eng. Fract. Mech. 89 (2012) 114–127.
[43] D. Mirzaei, R. Schaback, Direct meshless local Petrov–Galerkin (DMLPG) method: a generalized MLS approximation, Appl. Numer. Math. 68 (2013) 73–82.
[44] D. Mirzaei, R. Schaback, M. Dehghan, On generalized moving least squares and diffuse derivatives, IMA J. Numer. Anal. 32 (2012) 983–1000.
[45] D. Mirzaei, R. Schaback, Solving heat conduction problems by the direct meshless local Petrov–Galerkin (DMLPG) method, Numer. Algorithms 65 (2014) 275–291.
[46] A. Mazzia, G. Pini, F. Sartoretto, Numerical investigation on direct MLPG for 2D and 3D potential problems, CMES Comput. Model. Eng. Sci. 88 (2012) 183–210.
[47] B.Z. Lu, Y.C. Zhou, M.J. Holst, J.A. McCammon, Recent progress in numerical methods for the Poisson–Boltzmann equation in biophysical applications, Commun. Comput. Phys. 3 (2008) 973–1009.
[48] N. Sukumar, D.L. Chopp, N. Moes, T. Belytschko, Modeling holes and inclusions by level sets in the extended finite element method, Comput. Methods Appl. Mech. Engrg. 190 (2001) 6183–6200.
[49] R. Salehi, M. Dehghan, A generalized moving least square reproducing kernel method, J. Comput. Appl. Math. 249 (2013) 120–132.
[50] H. Wendland, Scattered Data Approximation, Cambridge University Press, 2005.
[51] S.N. Atluri, Z.D. Han, A.M. Rajendran, A new implementation of the meshless finite volume method, through the MLPG "mixed" approach, CMES Comput. Model. Eng. Sci. 6 (2004) 491–513.
[52] J.R. Xiao, M.A. McCarthy, A local Heaviside weighted meshless method for two-dimensional solids using radial basis functions, Comput. Mech. 31 (2003) 301–315.
[53] A. Mazzia, M. Ferronato, G. Pini, G. Gambolati, A comparison of numerical integration rules for the meshless local Petrov–Galerkin method, Numer. Algorithms 45 (2007) 61–74.
[54] C.T. Wu, Z. Li, M.C. Lai, Adaptive mesh refinement for elliptic interface problems using the non-conforming immersed finite element method, Int. J. Numer. Anal. Model. 8 (2011) 466–483.
[55] A.N. Marques, J.C. Nave, R.R. Rosales, A correction function method for Poisson problems with interface jump conditions, J. Comput. Phys. 230 (2011) 7567–7597.
[56] L. Mu, J. Wang, G. Wei, X. Ye, S. Zhao, Weak Galerkin methods for second order elliptic interface problems, J. Comput. Phys. 250 (2013) 106–125.
[57] M. Dehghan, A. Ghesmati, Combination of meshless local weak and strong (MLWS) forms to solve the two dimensional hyperbolic telegraph equation, Eng. Anal. Bound. Elem. 34 (2010) 324–336.
[58] M. Dehghan, A. Nikpour, The solitary wave solution of coupled Klein–Gordon–Zakharov equations via two different numerical methods, Comput. Phys. Commun. 184 (2013) 2145–2158.
[59] A. Mohebbi, M. Abbaszadeh, M. Dehghan, Compact finite difference scheme and RBF meshless approach for solving 2D Rayleigh–Stokes problem for a heated generalized second grade fluid with fractional derivatives, Comput. Methods Appl. Mech. Engrg. 264 (2013) 163–177.